 Human Molecular Genetics, 2000, Vol. 9, No. 2 155–163

ARTICLE

Retinal degeneration but not obesity is observed in null mutants of the tubby-like protein 1 gene

Sakae Ikeda, Nima Shiva[1], Akihiro Ikeda, Richard S. Smith, Steven Nusinowitz[2], Grace Yan[1], T. Richard Lin[1], Sunny Chu[1], John R. Heckenlively[2], Michael A. North[1], Jürgen K. Naggert, Patsy M. Nishina[+] and Mabel P. Duyao[1]

The Jackson Laboratory, 600 Main Street, Bar Harbor, ME 04609, USA, [1]AXYS Pharmaceuticals, Inc., La Jolla, CA 92037, USA and [2]Jules Stein Eye Institute, Los Angeles, CA 90095, USA

Received 20 August 1999; Revised and Accepted 5 November 1999

The *tub* gene is a member of a small, well conserved neuronal gene family of unknown function. Mutations within this gene lead to early-onset blindness and deafness, as well as late-onset obesity and insulin resistance. To test the hypothesis that mutations within other members of this gene family would lead to similar phenotypes as observed in tubby mice, and hence have similar functional properties, we have generated null mutants of the tubby-like protein (*Tulp*) 1 gene by homologous recombination. Similarly to tubby mice, *Tulp1*$^{-/-}$ mice exhibit an early-onset retinal degeneration with a progressive, rapid loss of photoreceptors, further supporting the notion that previously identified mutations within the human *TULP1* gene are indeed causative of retinitis pigmentosa. However, in contrast to tubby mice, *Tulp1*$^{-/-}$ mice exhibited normal hearing ability and, surprisingly, normal body weight despite the fact that both TUB and TULP1 are expressed in the same neurons within the hypothalamus in areas known to be involved in feeding behavior and energy homeo stasis. However, TUB and TULP1 show a distinctly different staining pattern in the nucleus of these neurons, perhaps explaining the difference in body weight between the *Tulp1*$^{-/-}$ and tubby mutant mice.

INTRODUCTION

tub, an autosomal recessive mutation, was originally described in 1990 (1). Tubby mice display a tripartite phenotype of blindness, deafness and maturity-onset obesity. Progressive retinal degeneration from apoptotic loss of photoreceptor cells, one of the first phenotypic abnormalities to be observed in mutant mice, results in abnormal electroretinograms detected as early as 3 weeks of age (2). Hearing loss, detected by auditory brainstem response analysis, is also abnormal by 3 weeks of age; however, degeneration of the inner hair cells in the cochlea is not observed at this age (3). Obesity, which precedes insulin resistance, is observable in males between 12 and 16 weeks, and in females ~2–4 weeks later (1). Interestingly, the obesity as well as the neurosensory phenotypes can be modified by genetic background to delay or suppress their expression (3, unpublished data).

tub was the last of the spontaneous, monogenic mouse obesity genes to be cloned. It encodes a novel and highly conserved protein that in the tubby mutant has a C-terminal deletion (4,5). The protein is strongly expressed in retina and brain (in particular the hypothalamus and hippocampus). The normal function of the tubby protein and the mechanism by which loss of function mutations lead to obesity or the other phenotypes are currently not known. Its expression in the hypothalamus nevertheless suggests that obesity in these mice may stem from aberrant signaling in the satiety centers of the brain.

tub is a member of a family of four genes, the tubby-like proteins (TULPs) (6,7). TULPs are characterized by a remarkably strong conservation of the C-terminal half of the protein, whereas the N-terminal portion is less strictly conserved. It may, therefore, be hypothesized that the *TULP* genes share a common function. However, they must in addition have acquired unique properties since the other gene family members that are expressed in the same tissues (as assessed by northern analysis) are obviously not able to compensate for the loss of *tub* function in tubby mice. Inability of the family members to compensate for one another may stem from their differential expression in specific cell types within each tissue (8). Nevertheless, strong C-terminal conservation and expression in both brain and eye raises the possibility that mutations in the related genes may cause similar syndromes as those observed in *tub*/*tub* mice.

Tulp1, like *tub*, shows strong expression in the eye. Based on its map location on human chromosome 6 and its structural similarity to TUB, we proposed TULP1 as a candidate gene for retinitis pigmentosa (RP) 14 (6). Indeed, associations of RP

[+]To whom correspondence should be addressed. Tel: +1 207 288 6384; Fax: +1 207 288 6079; Email: pmn@jax.org

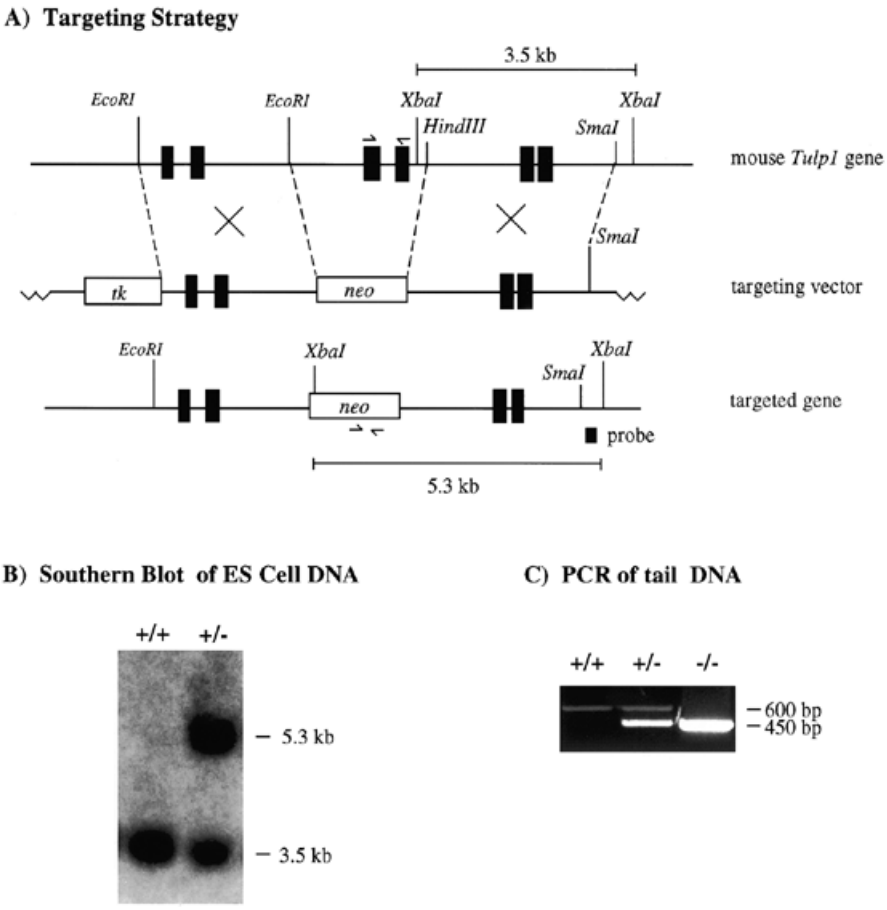

Figure 1. Generation of *Tulp1* null mice. (**A**) Gene targeting strategy. A fragment containing exons 8 and 9 of mouse *Tulp1* was replaced by the neo^r gene. (**B**) Southern blot analysis of *Xba*I-restricted genomic DNA derived from ES cell clones. The location of the 3′ probe used for the Southern blot analysis and the sizes of the *Xba*I fragments corresponding to wild-type and mutant alleles are shown. (**C**) PCR analysis of tail DNA. Dashes indicate the locations of the oligonucleotide primers used to detect the wild-type allele (600 bp) and the mutant allele (450 bp).

with mutations in human *TULP1* have been reported both in a large pedigree segregating for RP14 (9) as well as in sporadic cases of RP (10,11). Obesity and hearing loss have not been previously described as part of the phenotypic characteristics of these patients with RP. In order to ascertain whether *Tulp1* mutations do indeed lead to retinal degeneration in a co-isogenic background, as well as to test whether obesity and hearing loss are observed as a part of the phenotype, we created a mouse model by homologous recombination. In this communication, we describe the phenotype of *Tulp1* null mice.

RESULTS

Generation of *Tulp1* null mutant mice

A targeted disruption of *Tulp1* was generated through homologous recombination in embryonic stem (ES) cells (Fig. 1). After electroporation of the targeting vector (Fig. 1A), ES cell colonies were screened for the presence of the targeted allele by Southern hybridization (Fig. 1B), and chimeric mice were generated using the positive clones. One chimera that transmitted the targeted allele was backcrossed to C57BL/6 (B6) mice to produce heterozygotes, which then were intercrossed to produce homozygous animals (Fig. 1C). The absence of TULP1 protein in homozygous animals was confirmed by western blot analysis (Fig. 2A). Immunofluorescence using TULP1-N antibody also revealed no immunoreactivity for TULP1 in the retina of *Tulp1*$^{-/-}$ mice, whereas in wild-type control mice strong immunoreactivity was detected in the inner segments, perinuclear and synaptic regions of the photoreceptor cells (Fig. 2B).

Fundal examination

Fundi of 4- and 12-week-old *Tulp1*$^{-/-}$ mice were examined by indirect ophthalmoscopy and compared with those of *Tulp1*$^{+/+}$ littermates. *Tulp1*$^{-/-}$ mice exhibited attenuated retinal vessels and a granular appearing pigment epithelium. Similar observations were obtained at both time points studied.

Electroretinograms

Electroretinograms (ERGs) of *Tulp1*$^{-/-}$, *Tulp1*$^{+/-}$ and *Tulp1*$^{+/+}$ mice were recorded at 19, 32 and 67 days of age. Both rod and cone ERGs of *Tulp1*$^{-/-}$ mice were abnormal at the earliest age tested (19 days of age) with reduced a- and b-wave amplitudes compared with normal (Fig. 3). In addition, there is a progres-

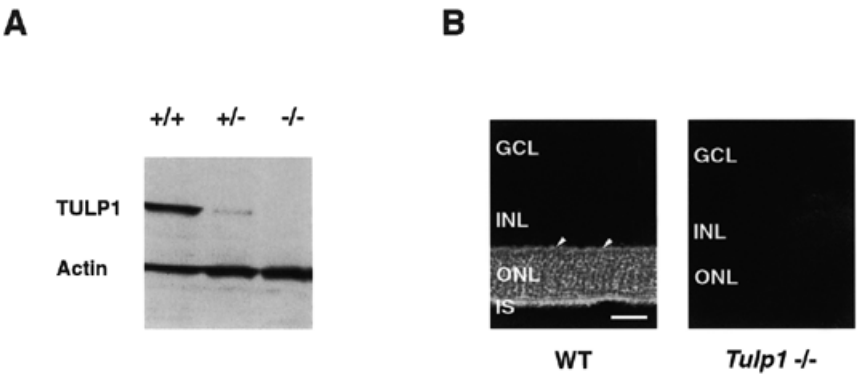

Figure 2. (**A**) Western blot analysis of TULP1. Proteins from retina and brain of *Tulp1*$^{+/+}$, *Tulp1*$^{+/-}$ and *Tulp1*$^{-/-}$ mice were detected using an anti-TULP1 polyclonal antibody. An anti-actin antibody was used as a positive control. (**B**) Immunofluorescence labeling of wild-type control and mutant retinas. In the wild-type retina, strong TULP1 immunoreactivity is observed in the inner segments, perinuclear and synaptic regions (arrowheads) of the photoreceptor cells. No immunoreactivity is present in the *Tulp1*$^{-/-}$ retina. GCL, ganglion cell layer; INL, inner nuclear layer; ONL, outer nuclear layer; IS, inner segments. Scale bar, 30 µm.

sive deterioration of rod and cone signals with age, with responses essentially non-detectable at 67 days of age (the oldest age tested). The similarity of waveforms for rod- and cone-mediated function at each age in the *Tulp1*$^{-/-}$ mice is consistent with the hypothesis that rod loss precedes cone loss and that residual function at the oldest ages is mediated by cones. *Tulp1*$^{+/+}$ and *Tulp1*$^{+/-}$ animals showed normal ERGs.

Histology of the retina

Light microscopic examination of the retina was performed at 2, 4, 6, 9, 12 and 20 weeks of age (Fig. 4). By 2 weeks of age, there was a shortening of the inner and outer segments (IS and OS, respectively) of photoreceptor cells in *Tulp1*$^{-/-}$ mice compared with *Tulp1*$^{+/+}$ littermates. However, the thickness of the outer nuclear layer (ONL) was comparable to that of control mice at this age. By 4 weeks of age, the thickness of the ONL was greatly reduced. Rapid, progressive loss of photoreceptor cells was observed, and by 12 weeks of age the ONL was reduced to a 1–2 nuclear layer thickness. By 20 weeks of age, some regions of the retina contained no apparent ONL, whereas other areas retained a 1–2 nuclear layer thickness. This variability appeared to be random and not associated with specific regions within the retina.

Electron microscopic examination was performed to characterize the abnormalities observed in *Tulp1*$^{-/-}$ mice further. As early as 2 weeks after birth, there were obvious photoreceptor abnormalities. The combined thickness of the IS and OS of the photoreceptors of *Tulp1*$^{-/-}$ mice was ~20% of normal. The OS were fragmented and distortion of the photoreceptor lamellae due to swelling was often observed (Fig. 5A). The photoreceptor IS also demonstrated fragmentation with the formation of isolated plasma membrane-bound vesicles that appeared to be either IS plasma membrane fragments or severely swollen extruded mitochondria (Fig. 5A, inset). Findings were similar, but more severe in 4-week-old *Tulp1*$^{-/-}$ mice, where many apoptotic nuclei were seen in the ONL (data not shown). Although present throughout the retina, the pathological changes observed varied in severity. The retinal pigment epithelium and the inner retina appeared normal.

Affected mice at 6 months of age demonstrated advanced retinal changes. Remnants of the external limiting membrane were in direct contact with the retinal pigment epithelium, and IS and OS of photoreceptors were absent. Only an occasional nucleus suggested photoreceptor origin. The outer plexiform layer had collapsed and could not be clearly delineated. The inner nuclear layer demonstrated moderately severe intracellular and mitochondrial swelling (Fig. 5B). However, in a few

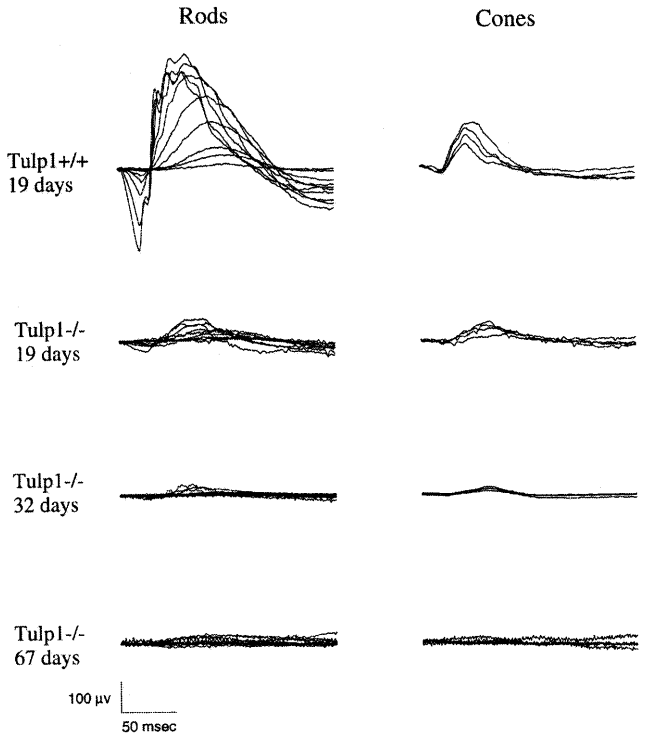

Figure 3. Representative rod (left) and cone (right) ERGs recorded from *Tulp1*$^{-/-}$ and wild-type mice. Records are shown for a control mouse at 19 days of age and for *Tulp1*$^{-/-}$ mice at 19, 32 and 67 days of age (top to bottom). Each panel shows the responses to a series of progressively higher intensities up to the maximum allowed by the photic stimulator (see the text for details). Both rod- and cone-mediated responses recorded from the *Tulp1*$^{-/-}$ mice are abnormal even at the earliest age tested (19 days of age) and are non-detectable by 67 days.

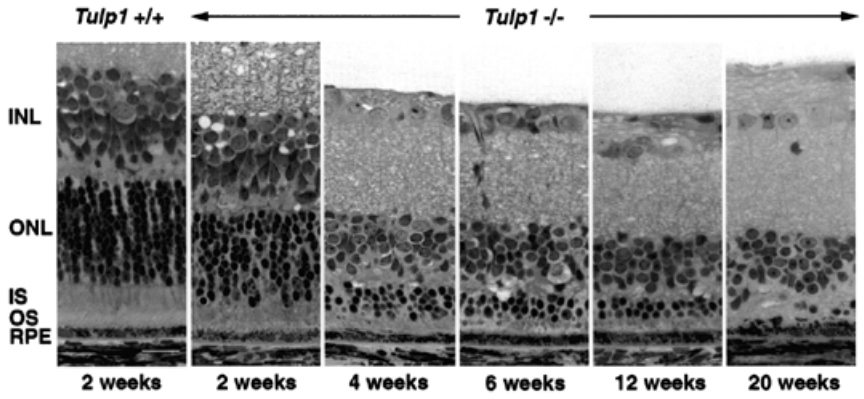

Figure 4. Light microscopy showing retinal degeneration in *Tulp1*$^{-/-}$ mice. A control section from a 2-week-old *Tulp1*$^{+/+}$ mouse is shown on the left. At 2 weeks of age, the shortening of the inner and outer segments of photoreceptor cells is apparent. By 4 weeks, the outer nuclear layer is greatly reduced. The degeneration is progressive over 20 weeks. INL, inner nuclear layer; ONL, outer nuclear layer; IS, inner segments; OS, outer segments; RPE, retinal pigment epithelium. Scale bar, 20 μm.

isolated areas of the retina the degeneration was not as severe (data not shown).

Terminal dUTP nick end labeling (TUNEL) assay

The TUNEL assay was performed in order to determine whether photoreceptor cell death in *Tulp1*$^{-/-}$ mice occurs through an apoptotic mechanism. At 18 days of age, numerous TUNEL-positive nuclei were observed in the ONL of *Tulp1*$^{-/-}$ mice (Fig. 6B), whereas only a few were observed in control mice (Fig. 6A). These apoptotic nuclei were scattered throughout the layer without aggregation, and surrounding nuclei appeared normal. At this age, the thickness of the ONL in *Tulp1*$^{-/-}$ mice was comparable to control mice.

Hearing test

Auditory brainstem response (ABR) analysis was performed to test the hearing ability of 4-week-old mice. Both *Tulp1*$^{-/-}$ and *Tulp1*$^{+/-}$ mice exhibited normal ABR thresholds across all four stimuli (click, 8, 16 and 32 kHz), indicating normal hearing ability.

Histology of the inner ear

Light microscopic examination of the cochlea was performed at 4 (Fig. 7) and 8 weeks of age. At both ages, no significant morphological difference was observed between the inner ear of *Tulp1*$^{-/-}$ mice and *Tulp1*$^{+/+}$ littermates, which is consistent with the result of the functional test for hearing ability.

Body weight gain

The body weight of *Tulp1*$^{-/-}$ and control (*Tulp1*$^{+/+}$ or *Tulp1*$^{+/-}$) mice was measured at 4, 6, 9, 12 and 20 weeks of age. These measurements were taken from at least three animals from each group of each gender at each time point. Body weight gain of *Tulp1*$^{-/-}$ mice was comparable to that of control mice (Fig. 8).

Expression of *Tulp1* in the brain

In order to determine whether *Tulp1* mRNA is expressed in the brain, reverse transcription–polymerase chain reaction (RT–PCR) assay was performed with mRNA from brains of *Tulp1*$^{+/+}$ and *Tulp1*$^{-/-}$ mice using primers specific for *Tulp1*. Expression of the *Tulp1* gene was detected in the brain of *Tulp1*$^{+/+}$, but not in *Tulp1*$^{-/-}$ mice (Fig. 9). The authenticity of the amplified *Tulp1* fragment was confirmed by Southern hybridization using a cDNA probe specific for the N-terminal half of *Tulp1*, as well as by sequencing.

Localization of TUB and TULP1 in the hypothalamus

In order to compare the expression patterns of TUB and TULP1 proteins in the hypothalamus, double labeling of brain sections of adult B6 mice was performed. In the paraventricular nucleus, TUB and TULP1 immunoreactivities were observed in the same cells. However, their subcellular localization differed. Intense TUB immunoreactivity was observed in the nucleolus of the nucleus, whereas TULP1 immunoreactivity was seen only within the nucleus as brightly staining grains (Fig. 10). The location of these grains coincided with larger regions diffusely labeled with 4′,6-diamidino-2-phenylindole (DAPI), suggesting that they might be chromatin-rich regions inside the nucleus. The arcuate, ventromedial and dorsomedial nuclei also showed the same patterns of expression of both proteins (data not shown). It should be noted that the expression level of TULP1 in the hypothalamus was significantly less compared with that in the photoreceptor cells in the retina.

DISCUSSION

Here we report the generation and phenotypic characterization of mice carrying null alleles of the *Tulp1* gene. Previously, nucleotide changes in the human *TULP1* gene have been found in patients with RP (9–11). With the exception of one large pedigree in which a point mutation in a splice junction of the *TULP1* gene was predicted to change 44 C-terminal amino acids (9), the remaining families were small nuclear kindreds with point mutations (10,11). Because humans are an outbred population, demonstrating an association of a polymorphism with a phenotype is not sufficient to prove causation. Our finding that incipient congenic stocks carrying a null mutation for *Tulp1* develop retinal degeneration provides evidence that a non-functional TULP1 protein can cause RP and supports the notion that the observed mutations in humans are causative.

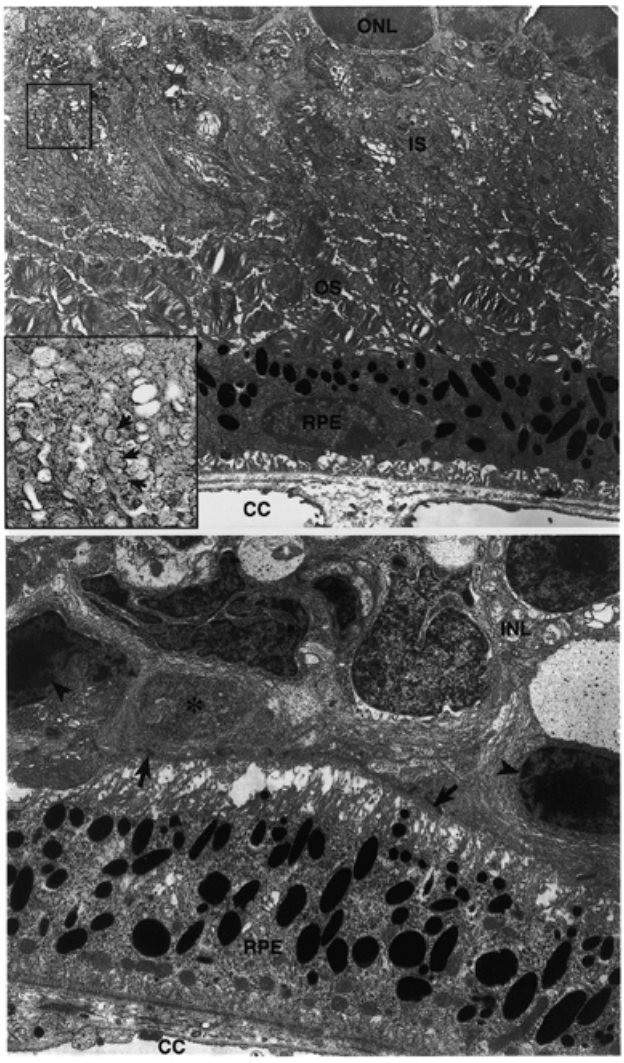

Figure 5. Electron microscopy showing the retina of *Tulp1*$^{-/-}$ mice. (**A**) *Tulp1*$^{-/-}$ mouse at 2 weeks of age. The choriocapillaris (CC) and the retinal pigment epithelium (RPE) are normal, as are the nuclei of the outer nuclear layer (ONL) in this field. The outer segments (OS) are fragmented and the entire outer segment layer is only 20% normal thickness. The inner segments (IS) are also fragmenting, as evidenced by the focal formation of vesicles in this area (inset, arrows). Magnification, 12 000×. Inset, ~36 000×. (**B**) *Tulp1*$^{-/-}$ mouse at 6 months of age. The CC and RPE are normal. Both IS and OS of the photoreceptors are absent, and the junctional complexes of the external limiting membrane (arrows) appear to be resting directly on the RPE. Two probable photoreceptor nuclei (arrowheads) are identified. A degenerating photoreceptor nucleus (*) is also present. The outer plexiform layer has collapsed and synaptic complexes cannot be identified. The cells of the inner nuclear layer (INL) lie close to the outer nuclear layer and many swollen cells are present. Magnification, 15 000×.

The retinal degeneration in *Tulp1*$^{-/-}$ mice resembles phenotypic characteristics reported for patients with RP14 in that it is early in onset and shows rapid progression (12). Both OS and IS in *Tulp1*$^{-/-}$ mice were abnormal by 2 weeks of age when fragmentation of both segments and the appearance of extracellular vesicular profiles within the region of the IS were observed. The abnormal accumulation of the vesicular profiles has also been reported in other retinal degeneration models such as tubby and Purkinje cell degeneration (*pcd*) mice (2,13). The suggestion that these vesicles

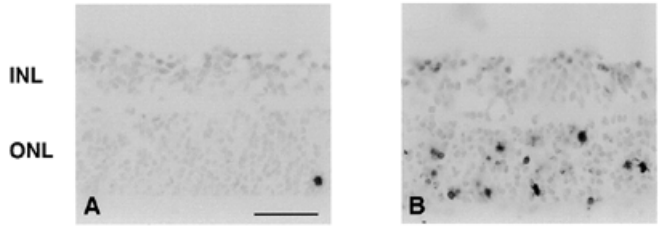

Figure 6. TUNEL staining of wild-type control and *Tulp1*$^{-/-}$ retina at 18 days of age. *Tulp1*$^{-/-}$ retina shows numerous TUNEL-positive nuclei in the outer nuclear layer (**B**), whereas control retina shows very few positively stained nuclei (**A**). INL, inner nuclear layer; ONL, outer nuclear layer. Scale bar, 30 μm.

may represent fragmented mitochondria is not unreasonable since we also show that the photoreceptor degeneration is due to apoptosis, and mitochondrial swelling is an early event in this process (14). These histological changes were paralleled by functional deficits. Electroretinograms of *Tulp1*$^{-/-}$ mice were severely affected with very low amplitudes of a- and b-waves in both light- and dark-adapted states, which were extinguished by 9 weeks of age.

In comparison with other mouse models for retinal degeneration, loss of photoreceptor cell bodies in *Tulp1*$^{-/-}$ mice was earlier than reported for tubby (*tub*) (2), retinal degeneration slow (*rds*, now *Prph*^{Rd2}) (15) or *pcd* (16) mice, but later than observed in retinal degeneration (*rd*, now *Pdeb*^{rd1}) (17), retinal degeneration 3 (*rd3*) (18) or retinal degeneration 4 (*Rd4*) (19) mice. The rate of reduction in ONL thickness in *Tulp1*$^{-/-}$ mice is rapid from 2 to 6 weeks of age, at which time only 2–3 rows of photoreceptor cell bodies are left, and proceeds more slowly thereafter. Rhodopsin null mutants, which have a similar time course for retinal degeneration, exhibit a more constant rate of photoreceptor cell body loss (20). Further investigation of *Tulp1*$^{-/-}$ mice, which display a distinct pattern of pathological abnormalities, together with other mutants may provide insights into molecules necessary for the normal function of the retina and into the mechanisms of retinal degeneration. It will be particularly useful in studying the pathogenesis of RP14.

The results of RT–PCR analysis show that *Tulp1* mRNA is expressed in the brain. This observation raises the possibility that TULP1, like TUB, may be expressed in the hypothalamus, which is known to be important for feeding behavior (21). Double labeling of brain sections with antibodies against TUB and TULP1 was performed in order to compare the localization of TUB and TULP1 in the hypothalamus. Both TUB and TULP1 show overlapping expression patterns in the arcuate and paraventricular nuclei of the hypothalamus as well as in the ventromedial hypothalamus. The present results appear to indicate that it is even the same set of neurons that are positive for both TUB and TULP1 proteins. It seems, therefore, surprising that *Tulp1*$^{-/-}$ mice showed normal body weight gains and that their final body weights did not differ from their heterozygous and wild-type littermate controls. These results may be explained by a difference observed in the nuclear staining patterns between TUB and TULP1. Whereas TUB was only detected in the nucleolus, TULP1 was present in structures that are likely to represent the perinucleolar cap (22) and coiled bodies (23) or gems (24) in the nucleus but not the nucleolus. Among the proposed functions of these nuclear organelles are ribosome assembly, and RNA processing and trafficking (23,25,26). It has become apparent that in neurons certain

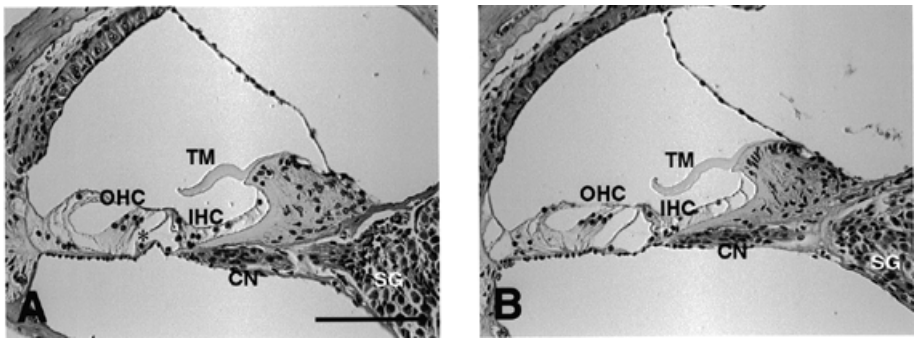

Figure 7. Light microscopy showing the cochlea of *Tulp1*$^{+/+}$ (**A**) and *Tulp1*$^{-/-}$ (**B**) mice. No morphological difference is observed between wild-type control and mutant animals. Separation of the arch of corti in (A) is artifactual (*). CN, cochlear nerve fibers; IHC, inner hair cells; OHC, outer hair cells; TM, tectorial membrane. Scale bar, 100 μm.

mRNAs and protein-synthesizing machinery are targeted to specific subcellular regions such as post-synaptic sites for local protein synthesis (27,28). The nuclear staining pattern observed here suggests then both a role for tubby-like proteins in this process, as well as a possible explanation for the different phenotypes observed in tubby versus *Tulp1*$^{-/-}$ mice. In such a scenario, TUB and TULP1 would be involved in the processing and/or trafficking of different sets of mRNAs and only the set associated with TUB encompasses mRNAs that are important in feeding behavior and/or energy homeostasis. The results presented here suggest new experimental avenues to pursue in the search for the functions of the *TULP* gene family.

MATERIALS AND METHODS

Generation of *Tulp1* null mutant mice

Mouse *Tulp1* genomic clones were isolated by screening a 129/Sv library (Stratagene, La Jolla, CA) using a fragment spanning bp 50–360 of human *TULP1* cDNA as a probe. The targeting vector was assembled using a 3′ 3.0 kb *Hin*dIII–*Sma*I and a 5′ 2.3 kb *Eco*RI fragment flanking exons 8 and 9 into the positive–negative selection vector pPNT (29). The targeting vector was linearized with *Not*I and transfected by electroporation into Rw4 ES cells (Genome Systems, St Louis, MO), which were derived from the 129/SvJ strain. Following positive and negative selection with G418 and ganciclovir, respectively, ES cell colonies were screened for homologous recombination by Southern blot analysis of DNA digested with *Xba*I. A 3′ external probe was used to detect a 3.5 kb wild-type band and a 5.3 kb mutant band. Of 79 ES clones analyzed, two were heterozygous for the targeted allele. Chimeras were generated from the ES cell lines, but only one transmitted the mutated allele. Heterozygous progeny were generated by backcrossing the chimera to wild-type C57BL/6 (B6) females. Homozygous animals were then derived from heterozygous matings and identified by PCR analysis of tail DNA using a forward primer in exon 8 (5′-CCTGTGGAAGTGGGTGAAC-3′) and a reverse primer in exon 9 (5′-GGTCACTGGAGAT-GAGATAGTTG-3′) and a pair of primers from the neo gene (5′-ACAATCGGCTGCTCTGATGC-3′ and 5′-GTCACGAC-GAGATCATCGC-3′). All four primers were used in a reaction containing ~10 ng of tail genomic DNA, 20 pmol each of the primers, 250 μM each of dNTP, 1 U of Expand *Taq* polymerase (Boehringer Mannheim, Indianapolis, IN), and buffer supplied by the manufacturer. PCR reactions were cycled 30 times at an annealing temperature of 57°C. Sizes of the wild-type and mutant PCR products are ~600 and 450 bp, respectively. The mice used in this study were either at third or fourth backcross generations to the B6 strain.

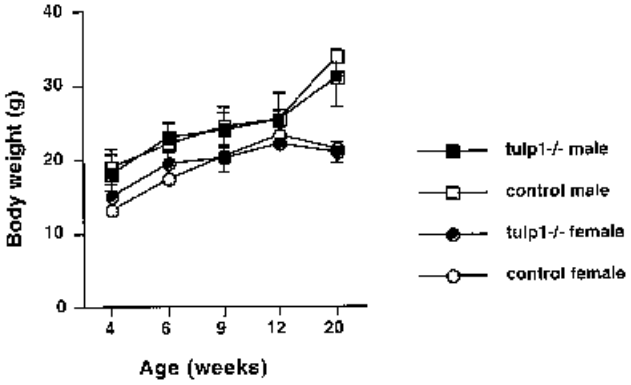

Figure 8. Growth curves of *Tulp1*$^{-/-}$ mice compared with littermate controls (*Tulp1*$^{+/+}$ or *Tulp1*$^{+/-}$). The body weight gain of *Tulp1*$^{-/-}$ mice is comparable to that of littermate controls.

Western blot analysis

Retina from wild-type (+/+), heterozygous (+/–) and homozygous (–/–) mice were isolated, homogenized and sonicated in 1× SDS–PAGE loading buffer. Solubilized proteins were then separated on 4–20% Tris–glycine gel (Novex, San Diego, CA), and transferred to PVDF membrane (Novex). The blots were blocked according to the Amersham ECL detection procedure, incubated with primary and peroxidase-conjugated secondary antibodies, and detected using chemiluminescent reagents (Amersham, Uppsala, Sweden). Rat polyclonal antiserum against the N-terminal half of TULP1 (TULP1-N) (8) was used to detect TULP1 protein. Anti-actin antibody (Sigma, St Louis, MO) was used as a control antibody.

Clinical examination

Eyes of mice were dilated with atropine prior to examination by indirect ophthalmoscopy with a 60 or 78 diopter aspheric

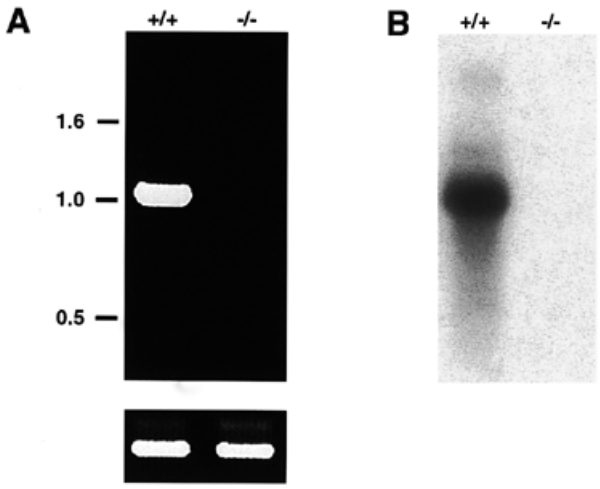

Figure 9. Expression of *Tulp1* in the brain assessed by RT–PCR analysis. The product of expected size (1.1 kb) was detected in the brain of *Tulp1*$^{+/+}$, but not in *Tulp1*$^{-/-}$ mice (**A**, top panel). The β-actin control (540 bp) was amplified equally in both animals (A, bottom panel). The authenticity of the amplified *Tulp1* fragment was confirmed by Southern hybridization (**B**) of a blot prepared from the gel in (A) and probed with an N-terminal *Tulp1* cDNA probe.

lens. Fundus photographs were taken with a Kowa Genesis fundus camera (Kowa, Tokyo, Japan) using a Volk superfield lens (Volk Optical, Mentor, OH) held 2 inches from the eye. High flash intensity was used with Kodak 200ASA color slide film (Eastman Kodak, Rochester, NY) (30).

Electroretinography

Mice were dark adapted for 2 h and anesthetized prior to testing with an intraperitoneal injection of normal saline solution containing ketamine (15 mg/g body wt) and xylazine (7 mg/g body wt). The right eye of each mouse was dilated (0.5% cyclopentolate hydrochloride and 2.5% phenylephrine hydrochloride) to a maximum diameter of 2.0 mm. ERGs were recorded using a gold loop electrode placed on the corneal surface at the limbus and referenced to a gold wire in the mouth. A needle electrode inserted in the tail served as ground. Signals were amplified (×10 000, CP511 AC amplifier; Grass Instruments, Warwick, RI), sampled every 0.8 ms with the A/D board (PCI-1200; National Instruments, Austin, TX) in a personal computer, and averaged. Low- and high-frequency cut-offs were set at 1 and 1000 Hz, respectively.

All stimuli were presented in a Ganzfeld dome painted with a highly reflective matte paint (#6080; Eastman Kodak). Rod-mediated ERGs were recorded to short-wavelength (Wratten 47A; λ_{max} = 470 nm) flashes that were varied over a 4.0 log unit range of intensities up to the maximum allowable by the phototic stimulator (PS33 Plus; Grass Instruments). Cone-mediated responses were obtained with white flashes on a rod-saturating background after 10 min of light adaptation. Responses were computer averaged at all intensities with up to 50 records averaged for the weakest signals. A signal rejection window was used to eliminate electrical artifacts produced by blinking and eye movements.

ABR analysis

A computer-aided evoked potential system (Intelligent Hearing System, Miami, FL) was used to test mice for ABR thresholds as previously described by Zheng *et al*. (31). Mice were tested with click stimuli and also with 8, 16 and 32 kHz tone pips at varying intensity, from low to high (10–90 dB sound pressure level).

Light microscopy

Mice were killed by carbon dioxide asphyxiation at 2, 4, 6, 9, 12 and 20 weeks of age. Enucleated eyes were placed in ice-cold fixative (1% paraformaldehyde/2% glutaraldehyde/0.1 M cacodylate) for 48 h, embedded in hydroxyethylmethacrylate, and sectioned in a plane to include the ora serrata and optic nerve. Sections were stained with hematoxylin and eosin.

For histology of the inner ear, mice were killed by carbon dioxide asphyxiation at 4 and 8 weeks of age. Cochleae were removed and placed in Bouin's fixative for 10 h, followed by

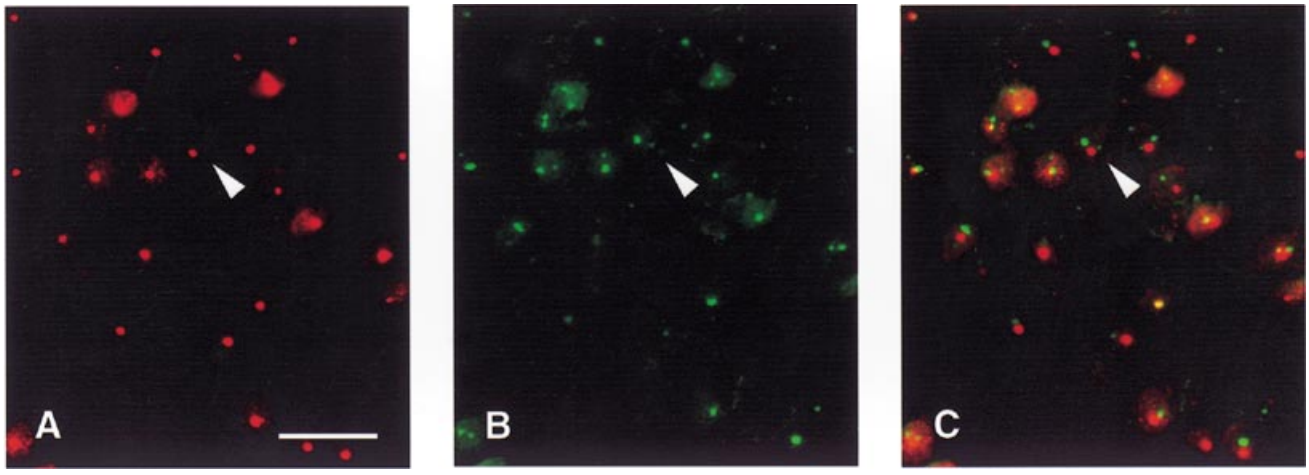

Figure 10. Immunofluorescence micrographs of the paraventricular nucleus in the hypothalamus of C57BL/6 mice after double labeling with antibodies against TUB [red (**A**)] and TULP1 [green (**B**)]. (**C**) A 'merged' version of (A) and (B). Intense TUB staining is observed in the nucleolus (A), whereas TULP1 immunoreactivity is observed as distinct grains in the nucleus (B). Note that although both proteins are expressed in the nucleus of the same cell, they localize to different structures in the nucleus, as indicated by the absence of orange/yellow staining [arrowheads, compare (A)–(C)]. Scale bar, 30 μm.

incubation in decalcifying solution (Cal-Ex; Fisher, Suwanee, GA) for 12 h. After embedding in paraffin, serial sections were cut and stained with hematoxylin and eosin.

Immunofluorescence

Two-week-old *Tulp1*$^{-/-}$ and wild-type control mice were killed by carbon dioxide asphyxiation. Eyes were enucleated and placed in 4% paraformaldehyde (PFA) in phosphate-buffered saline (PBS) for 3 h, dehydrated, and embedded in paraffin. A minimum of three eyes from different animals in each group were used for this experiment. Sections of 6 μm thickness were cut and mounted on slides pre-treated with Vectabond (Vector Laboratories, Burlingame, CA). Sections were heated in the microwave for 8 min in sodium citrate buffer pH 6.5 for antigen retrieval and then incubated overnight with rat polyclonal antiserum against the N-terminal half of TULP1 (TULP1-N) (8) at a dilution of 1:2000. Antibody binding was detected using biotinylated donkey anti-rat IgG (1:200; Vector Laboratories) followed by fluorescein isothiocyanate (FITC)–Avidin D. Nuclear counterstaining was performed with DAPI at a final concentration of 5 μg/ml. Images were collected on a Leica DMRXE fluorescent microscope (Leica, Deerfield, IL) equipped with a SPOT CCD camera (Diagnostic Instruments, Sterling Heights, MI) using appropriate bandpass filters for each fluorochrome.

For double labeling of brain sections, adult B6 mice were anesthetized with tribromoethanol and perfused with PBS followed by 4% PFA in PBS. Brains were dissected out and post-fixed in the same fixative for 1–3 h, dehydrated, and embedded in paraffin. Sections of 6 μm thickness were cut and mounted on slides pre-treated with poly-L-lysine (Sigma). Sections were subjected to antigen retrieval as described above, incubated with rabbit polyclonal antiserum against the N-terminal half of TUB (Tub-N2) (1:300) (8), and then with TULP1-N (1:200). Antibody binding was detected using biotinylated donkey anti-rat IgG followed by FITC–Avidin D, or Cy3-conjugated donkey anti-rabbit IgG (Jackson Immunoresearch, West Grove, PA). Nuclear counterstaining and image analysis were performed as described above.

Electron microscopy

The eyes were removed immediately after carbon dioxide euthanasia and fixed for 3 h in a cold, buffered glutaraldehyde–PAF mixture (32). After 3 h, the anterior segment was removed and the posterior segment cut into 1 × 2 mm blocks of retina, choroid and sclera. The additional fixation of the whole eye before dissection improved adhesion of the retina to the pigment epithelium and did not alter the quality of preservation. The dissected tissue was placed in fresh fixative for an additional 2–8 h and was post-fixed in 1% osmium tetroxide, dehydrated, and embedded in plastic. Thick sections were cut for orientation and thin sections cut and stained with uranyl acetate and lead citrate, and examined in a transmission electron microscope.

TUNEL assay

Eighteen-day-old *Tulp1*$^{-/-}$ and wild-type (+/+) control mice were killed by carbon dioxide asphyxiation. Eyes were enucleated and placed in 10% neutral buffered formalin for 20 h, dehydrated, and embedded in paraffin. Three eyes from different animals in each group were assayed per time point. Sections were prepared in the manner described earlier. Slides were treated with proteinase K (20 μg/ml) in PBS for 15 min at room temperature and washed four times for 2 min in distilled water. The TUNEL assay was carried out using the Apop Tag *in situ* Apoptosis Detection kit (Oncor, Gaithersburg, MD). For a negative control, water was substituted for the terminal deoxynucleotidyl transferase (TdT) enzyme in the reaction buffer of the kit.

RT–PCR analysis

Poly(A)$^+$ RNA (1 μg) extracted from the brain of *Tulp1*$^{+/+}$ and *Tulp1*$^{-/-}$ mice was treated with DNase I (Boehringer Mannheim) and reverse transcribed using the Superscript preamplification system (Gibco BRL, Grand Island, NY). PCR was performed using 5 ng of single-stranded DNA, a *Tulp1* forward primer (5′-CTGCAGGAGGAGACCCTTCG-3′), a reverse primer (5′-CCGATGAAATTCTCGCCTC-3′) and Expand (Boehringer Mannheim). Forward and reverse β-actin oligomers were 5′-GTGGGCCGCTCTAGGCACCAA-3′ and 5′-CTCTTTGATGTCACGCACGATTTC-3′, respectively. PCR reactions were cycled 40 times at an annealing temperature of 58°C. PCR products were electrophoresed, transferred to a nylon membrane and hybridized with ^{32}P-random-labeled DNA probe for *Tulp1* (8). This probe is specific for the N-terminal coding sequence of *Tulp1* and encompasses the two exons that were removed by homologous recombination. Brains from three animals of each group (*Tulp1*$^{+/+}$ and *Tulp1*$^{-/-}$) were used for the experiments and yielded the same result.

ACKNOWLEDGEMENTS

We thank Jennifer Le, Jane Morrow and Dawn Braun for their help with the breeding and maintenance of the mutant mice; Dr Bo Chang, Norman L. Hawes, Ronald E. Hurd for fundal examination and ERG recording; Dr Asif Azimi for ERG recording; Dr Qing Yin Zheng for ABR analysis; Philip Rosenstiel for excellent advice on immunofluorescence; and Irina Sorokina, Ying Zhao, Deborah Boswell Lane and Lesley S. Bechtold for technical assistance. We are also grateful to Drs Thomas Gridley, Gregory A. Cox and Barbara B. Knowles for carefully reviewing the manuscript. This work was supported by grants from the Foundation for Fighting Blindness, AXYS Pharmaceuticals and the National Eye Institute, EY11996. Institutional shared services were supported by National Cancer Institute Cancer Center grant CA-34196.

REFERENCES

1. Coleman, D.L. and Eicher, E.M. (1990) Fat (fat) and tubby (tub): two autosomal recessive mutations causing obesity syndromes in the mouse. *J. Hered.*, **81**, 424–427.
2. Heckenlively, J.R., Chang, B., Erway, L.C., Peng, C., Hawes, N.L., Hageman, G.S. and Roderick, T.H. (1995) Mouse model for Usher syndrome: linkage mapping suggests homology to Usher type I reported at human chromosome 11p15. *Proc. Natl Acad. Sci. USA*, **92**, 11100–11104.
3. Ikeda, A., Zheng, Q.Y., Rosenstiel, P., Maddatu, T., Zuberi, A.R., Roopenian, D.C., North, M.A., Naggert, J.K., Johnson, K.R. and Nishina, P.M. (1999) Genetic modification of hearing in tubby mice: evidence for the existence of a major gene (*moth1*) which protects tubby mice from hearing loss. *Hum. Mol. Genet.*, **8**, 1761–1767.

4. Noben-Trauth, K., Naggert, J.K., North, M.A. and Nishina, P.M. (1996) A candidate gene for the mouse mutation tubby. *Nature*, **380**, 534–538.
5. Kleyn, P.W., Fan, W., Kovats, S.G., Lee, J.J., Pulido, J.C., Wu, Y., Berkemeier, L.R., Misumi, D.J., Holmgren, L., Charlat, O. *et al*. (1996) Identification and characterization of the mouse obesity gene *tubby*: a member of a novel gene family. *Cell*, **85**, 281–290.
6. North, M.A., Naggert, J.K., Yan, Y., Noben-Trauth, K. and Nishina, P.M. (1997) Molecular characterization of *TUB*, *TULP1*, and *TULP2*, members of the novel tubby gene family and their possible relation to ocular diseases. *Proc. Natl Acad. Sci. USA*, **94**, 3128–3133.
7. Nishina, P.M., North, M.A., Ikeda, A., Yan, Y. and Naggert, J.K. (1998) Molecular characterization of a novel tubby gene family member, *TULP3*, in mouse and humans. *Genomics*, **54**, 215–220.
8. Ikeda, S., He, W., Ikeda, A., Naggert, J.K., North, M.A. and Nishina, P.M. (1999) Cell specific expression of tubby gene family members in the retina. *Invest. Ophthalmol. Vis. Sci.*, **40**, 2706–2712.
9. Banerjee, P., Kleyn, P.W., Knowles, J.A., Lewis, C.A., Ross, B.M., Parano, E., Kovats, S.G., Lee, J.J., Penchaszadeh, G.K., Ott, J. *et al.* (1998) TULP1 mutation in two extended Dominican kindreds with autosomal recessive retinitis pigmentosa. *Nature Genet.*, **18**, 177–179.
10. Hagstrom, S.A., North, M.A., Nishina, P.M., Berson, E.L. and Dryja, T.P. (1998) Recessive mutations in the gene encoding the tubby-like protein TULP1 in patients with retinitis pigmentosa. *Nature Genet.*, **18**, 174–176.
11. Gu, S., Lennon, A., Li, Y., Lorenz, B., Fossarello, M., North, M.A., Gal, A. and Wright, A. (1998) Tubby-like protein-1 mutations in autosomal recessive retinitis pigmentosa. *Lancet*, **351**, 1103–1104.
12. Lewis, C.A., Batlle, I.R., Batlle, K.G.R., Banerjee, P., Cideciyan, A.V., Huang, J., Aleman, T.S., Huang, Y., Ott, J., Gilliam, T.C. *et al.* (1999) Tubby-like protein 1 homozygous splice-site mutation causes early-onset severe retinal degeneration. *Invest. Ophthalmol. Vis. Sci.*, **40**, 2106–2114.
13. Blanks, J.C., Mullen, R.J. and LaVail, M.M. (1982) Retinal degeneration in the *pcd* cerebellar mutant mouse. II. Electron microscopic analysis. *J. Comp. Neurol.*, **212**, 231–246.
14. Wallace, D.C. (1999) Mitochondrial diseases in man and mouse. *Science*, **283**, 1482–1488.
15. Sanyal, S., DeRuiter, A. and Hawkins, R.K. (1980) Development and degeneration of retina in *rds* mutant mice: light microscopy. *J. Comp. Neurol.*, **194**, 193–207.
16. LaVail, M.M., Blanks, J.C. and Mullen, R.J. (1982) Retinal degeneration in the *pcd* cerebellar mutant mouse. I. Light microscopic and autoradiographic analysis. *J. Comp. Neurol*., **212**, 217–230.
17. LaVail, M.M. (1981) Analysis of neurological mutants with inherited retinal degeneration. Friedenwald lecture. *Invest. Ophthalmol. Vis. Sci*., **21**, 638–657.
18. Chang, B., Heckenlively, J.R., Hawes, N.L. and Roderick, T.H. (1993) New mouse primary retinal degeneration (*rd-3*). *Genomics*, **16**, 45–49.
19. Roderick, T.H., Chang, B., Hawes, N.L. and Heckenlively, J.R. (1997) A new dominant retinal degeneration (*Rd4*) associated with a chromosomal inversion in the mouse. *Genomics*, **42**, 393–396.
20. Humphries, M.M., Rancourt, D., Farrar, G.J., Kenna, P., Hazel, M., Bush, R.A., Sieving, P.A., Sheils, D.M., McNally, N., Creighton, P. *et al*. (1997) Retinopathy induced in mice by targeted disruption of the rhodopsin gene. *Nature Genet.*, **15**, 216–219.
21. Kalra, S.P., Dube, M.G., Pu, S., Xu, B., Horvath, T.L. and Kalra, P.S. (1999) Interacting appetite-regulating pathways in the hypothalamic regulation of body weight. *Endocr. Rev.*, **20**, 68–100.
22. Ghetti, A., Pinol-Roma, S., Michael, W.M., Morandi, C. and Dreyfuss, G. (1992) hnRNP I, the polypyrimidine tract-binding protein: distinct nuclear localization and association with hnRNAs. *Nucleic Acids Res.*, **20**, 3671–3678.
23. Matera, A.G. (1999) Nuclear bodies: multifaceted subdomains of the interchromatin space. *Trends Cell Biol.*, **9**, 302–309.
24. Matera, A.G. and Frey, M.R. (1998) Coiled bodies and gems: janus or gemini? *Am. J. Hum. Genet.*, **63**, 317–321.
25. Gall, J.G., Tsvetkov, A., Wu, Z. and Murphy, C. (1995) Is the sphere organelle/coiled body a universal nuclear component? *Dev. Genet.*, **16**, 25–35.
26. Huang, S., Deernick, T.J., Ellisman, M.H. and Spector, D.L. (1998) The perinucleolar compartment and transcription. *J. Cell Biol.*, **143**, 35–47.
27. Steward, O. (1997) mRNA localization in neurons: a multipurpose mechanism? *Neuron*, **18**, 9–12.
28. Gardiol, A., Racca, C. and Triller, A. (1999) Dendritic and postsynaptic protein synthetic machinery. *J. Neurosci*., **19**, 168–179.
29. Tybulewicz, V.L., Crawford, C.E., Jackson, P.K., Bronson, R.T. and Mulligan, R.C. (1991) Neonatal lethality and lymphopenia in mice with a homozygous disruption of the c-abl proto-oncogene. *Cell*, **65**, 1153–1163.
30. Hawes, N.L., Smith, R.S., Chang, B., Davisson, M., Heckenlively, J.R. and John, S.W. (1999) Mouse fundus photography and angiography: a catalogue of normal and mutant phenotypes. *Mol. Vis.*, **15**, 5–22.
31. Zheng, Q.Y., Johnson, K.R. and Erway, L.C. (1999) Assessment of hearing in 80 inbred strains of mice by ABR threshold analyses. *Hearing Res.*, **130**, 94–107.
32. Smith, R.S. and Rudt, L.A. (1973) Ultrastructural studies of the blood–aqueous barrier. *Am. J. Ophthalmol*., **76**, 937–947.